ACS OMEGA

http://pubs.acs.org/journal/acsodf

Article

From CO_2 to DME: Enhancement through Heteropoly Acids from a Catalyst Screening and Stability Study

Dustin Kubas, Jennifer Maria Beck, Erdogan Kasisari, Timo Schätzler, Anita Becherer, Anna Fischer, and Ingo Krossing*

Cite This: *ACS Omega* 2023, 8, 15203−15216

Read Online

ACCESS | Metrics & More | Article Recommendations | Supporting Information

ABSTRACT: The direct synthesis of dimethyl ether (DME) *via* CO_2 hydrogenation in a single step was studied using an improved class of bifunctional catalysts in a fixed bed reactor (T_R: 210−270 °C; 40 bar; gas hourly space velocity (GHSV) 19,800 NL kg_{cat}^{-1} h^{-1}; ratio $CO_2/H_2/N_2$ 3:9:2). The competitive bifunctional catalysts tested in here consist of a surface-basic copper/zinc oxide/zirconia (CZZ) methanol-producing part and a variable surface-acidic methanol dehydration part and were tested in overall 45 combinations. As dehydration catalysts, zeolites (ferrierite and β-zeolite), alumina, or zirconia were tested alone as well as with a coating of Keggin-type heteropoly acids (HPAs), i.e., silicotungstic or phosphotungstic acid. Two different mixing methods to generate bifunctional catalysts were tested: (i) a single-grain method with intensive intra-particular contact between CZZ and the dehydration catalyst generated by mixing in an agate mortar and (ii) a dual-grain approach relying on physical mixing with low contact. The influence of the catalyst mixing method and HPA loading on catalyst activity and stability was investigated. From these results, a selection of best-performing bifunctional catalysts was investigated in extended measurements (time on stream: 160 h/7 days, T_R: 250 and 270 °C; 40 bar; GHSV 19,800 NL kg_{cat}^{-1} h^{-1}; ratio $CO_2/H_2/N_2$ 3:9:2). Silicotungstic acid-coated bifunctional catalysts showed the highest resilience toward deactivation caused by single-grain preparation and during catalysis. Overall, HPA-coated catalysts showed higher activity and resilience toward deactivation than uncoated counterparts. Dual-grain preparation showed superior performance over single grain. Furthermore, silicotungstic acid coatings with 1 KU nm^{-2} (Keggin unit per surface area of carrier) on Al_2O_3 and ZrO_2 as carrier materials showed competitive high activity and stability in extended 7-day measurements compared to pure CZZ. Therefore, HPA coating is found to be a well-suited addition to the CO_2-to-DME catalyst toolbox.

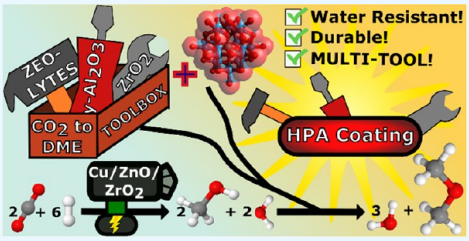

INTRODUCTION

The use of fossil resources has increased the amount of carbon dioxide (CO_2) in the atmosphere, leading to a pronounced greenhouse effect. Thus, using CO_2 together with green hydrogen (H_2) as a feedstock is a promising nontoxic and low-cost path toward a sustainable and green chemical industry.[1−5] CO_2-based C_1 chemicals can help to reduce global warming and fossil resource depletion by closing the carbon cycle.[6−9] In addition, the use of CO_2 for renewable fuels, such as dimethyl ether (DME), may be an attractive method to further address these problems.[6,10,11]

Thermodynamic Considerations to DME Synthesis Starting from CO_2 Hydrogenation. A CO_2-based platform molecule is methanol (MeOH). It can be produced in exothermic reactions from H_2 and CO_2 (CO_2-to-MeOH, in short CtM; Table 1) or CO (Syngas-to-MeOH, in short StM). Starting from CO_2, stoichiometric amounts of water are produced. Further, as a side reaction, the endothermic reverse water gas shift (RWGS) reaction competes for the CO_2 and the valuable H_2 feed, forming CO and water. CtM is slightly endergonic at standard conditions due to its volume-reducing nature. Combined with the RWGS reaction, a thermodynamic

Table 1. Energetics of the Reaction Network

name	abbr.	occurring reactions (gas phase)	$\Delta_r H^{298K}$ ($\Delta_r G^{298K}$)/kJ mol^{-1}
CO_2 hydrogenation	CtM	$CO_2 + 3\ H_2 \rightleftharpoons CH_3OH + H_2O$	−49 (+3.8)
CO hydrogenation	StM	$CO + 2\ H_2 \rightleftharpoons CH_3OH$	−90 (−25)
reverse water gas shift	RWGS	$CO_2 + H_2 \rightleftharpoons CO + H_2O$	+41 (+29)
MeOH dehydration	MtD	$2\ H_3COH \rightleftharpoons H_3COCH_3 + H_2O$	−25 (−17)
name	abbr.	overall reactions	$\Delta_r H^{298K}$ ($\Delta_r G^{298K}$)/ kJ mol^{-1}
CO_2 to DME	CtD	$2\ CO_2 + 6\ H_2 \rightleftharpoons H_3COCH_3 + 3H_2O$	−123 (−9.6)
CO to DME	StD	$2\ CO + 4\ H_2 \rightleftharpoons H_3COCH_3 + H_2O$	−205 (−67)

Received: January 11, 2023
Accepted: March 27, 2023
Published: April 21, 2023

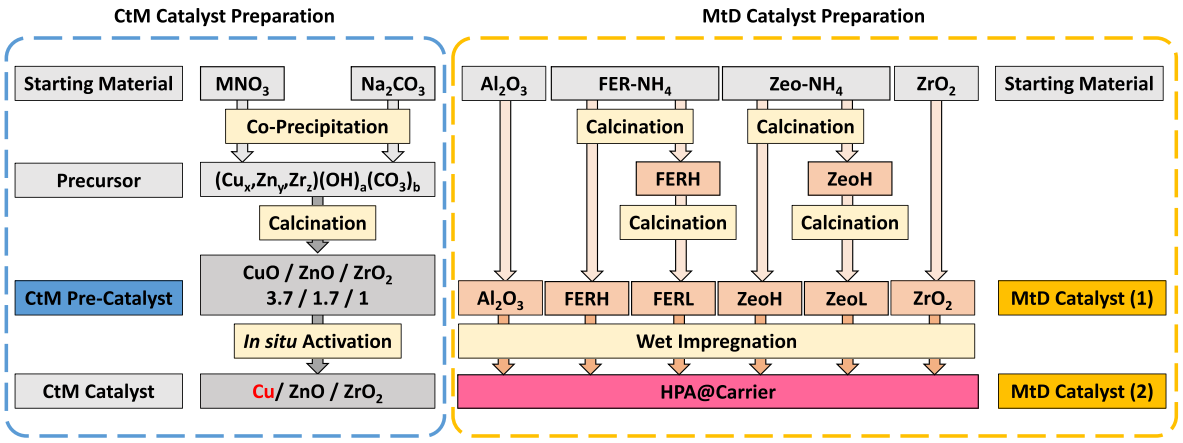

Figure 1. Synthesis scheme of the CtM catalyst (left) and MtD catalysts (right). Materials used for the preparation of the bifunctional catalysts are highlighted in blue (CtM pre-catalyst) and orange (MtD catalysts 1 and 2).

limitation to the CO_2 conversion is set. This limit can be increased, if the MeOH formed is directly dehydrated to DME (MeOH-to-DME, in short MtD).[12,13] The overall energetics is given for CO_2/H_2 (CO_2-to-DME, in short CtD) and CO/H_2 (Syngas-to-DME, StD).

When pure CO_2 or CO_2-rich feedstock is used, the main obstacles are defined by this reaction network. Hence, the catalyst systems used must cope with the high abundance of water and with the endothermic RWGS reaction, which competes for the green hydrogen feedstock.[14−16] These limitations define the main tasks in catalyst design: preparing water tolerant, highly active, and stable catalyst systems. DME synthesis needs two separate catalysts: one hydrogenation catalyst part to form MeOH (the CtM catalyst) and one solid acid catalyst part to perform the dehydration (the MtD catalyst). Together, they form a bifunctional catalyst system. Surface-basic $Cu/ZnO/ZrO_2$ (CZZ) hydrogenation catalysts for MeOH synthesis are reported to be more water tolerant than the industrial (syngas) favorite $Cu/ZnO/Al_2O_3$ (CZA).[17−21] Water, if adsorbed, blocks active sites and accelerates deactivation through particle sintering.[22−24] The industrially dominant two-step DME process uses γ-Al_2O_3 as the dehydration catalyst. γ-Al_2O_3 is a Lewis acidic material, which has tendencies to strongly adsorb water, resulting in the loss of its dehydration capacities, if applied to CtD. This process can be described as "drowning". In comparison, Brønsted sites are more tolerant toward water.[25] Therefore, Brønsted acidic zeolites like ferrierites, beta zeolites, and H-ZSM-5-type zeolites are in the focus of research for the CtD reaction.[26−28] Side reactions and deactivation through coking are often mentioned disadvantages of zeolites.[29,30] For the MtD, high-surface-area materials can be coated with Brønsted acids. Rojas et al., Schnee et al., and Kozhevnikov et al. reported tungstosilicic acid and phosphotungstic acid, both Keggin-type heteropoly acids, as suitable coating materials for the gaseous MtD reaction.[31−37] Navarro et al. reported the effective use of bifunctional catalysts with heteropoly acid (HPA) coating in the direct DME synthesis from syngas.[38,39] For the StD reaction, even core−shell structured catalysts with an HPA-impregnated γ-Al_2O_3 and a CZA core are reported.[40] Since Keggin-type polyacids have a well-defined structure with a footprint of estimated 1 nm^2, the amount of Keggin units (KU) per surface area of carrier material can be calculated as Keggin unit loading (KU nm^{-2}).

For the generation of bifunctional catalysts, several methods are published.[26,27,39−45] The defining factor is the degree of spatial proximity between the two catalyst functions. High degree of proximity between the MeOH-producing sites and DME-producing sites is kinetically beneficial, as the reactions are consecutive and short distance equal faster reaction rates. However, high proximity of surface-basic CtM and surface-acidic MtD catalysts can lower the catalyst system's life span.[22,29,39,46,47]

In our recent study, the limit of CtD for CO_2 conversion and yield of valuable products was found to be higher by up to 20% (conversion)/70% (yield) than for sole CtM, if performed under thermodynamic control. This indicates that under the thermodynamic regime, CtD has great potential for CO_2 valorization. However, to distinguish good from poor catalyst materials, reaction conditions must be set in a regime where thermodynamics and kinetics are competing for dominance.[48] Under thermodynamic control, CO_2 conversions and product yields of 30 and 21% were achieved, while under kinetic control, apparent activation energies of as low as 42 kJ mol^{-1} were determined. In this work, the influence of the preparation method and HPA loading on catalyst activity and stability is investigated. Catalysis tests were performed at reaction temperatures T_R between 210 and 270 °C at 40 bar pressure (GHSV 19,800 NL kg_{cat}^{-1} h^{-1}; ratio $CO_2/H_2/N_2$ 3:9:2). These conditions have shown to be neither dominated by thermodynamics nor kinetics. Thus, they pose demanding reaction conditions suitable to distinguish good from poor catalysts. From these results, a selection of promising bifunctional catalysts was investigated in extended 7-day measurements at T_R = 250 and 270 °C, with the other conditions kept constant.

EXPERIMENTAL AND METHOD SECTION

Methods. A $Cu/ZnO/ZrO_2$ (CZZ) catalyst, which has been optimized over the last 10 years in our group and is on par with commercial systems, was used as the hydrogenation component (CtM catalyst).[48−50] Here, 18 single batches of each 5 g were combined to form a single homogeneous large batch. Several dehydration catalysts (variants of β-zeolite and ferrierite, alumina, zirconia, as well as heteropolyacids, i.e., silicotungstic or phosphotungstic acid, coated versions thereof) were tested. The dehydration component (MtD catalyst) was mixed in two distinctly different ways with the hydrogenation

https://doi.org/10.1021/acsomega.3c00149
ACS Omega 2023, 8, 15203−15216

catalyst (CtM catalyst) to obtain the bifunctional catalyst for direct DME synthesis. Mixing methods were designed either to result in high intra-particular interfaces or to avoid direct contact of the two catalyst functions. The first method is named "homogeneous" and is done by thoroughly mixing CtM and MtD catalysts' primary particles in an agate mortar, followed by pressing and sieving to particle sizes of 100−200 μm. This method results in mixed, secondary particles or "single grain" bifunctional catalyst systems. The "heterogeneous" method consists in physically mixing secondary particles (100−200 μm) of pure CtM and pure MtD catalysts, resulting in "dual grain" bifunctional catalysts. The standard testing procedure includes a temperature program starting at T_1 = 250 °C, T_2 = 230 °C, T_3 = 210 °C, T_4 = 270 °C, ending at T_5 = 250 °C to measure deactivation with a constant pressure (40 bar), a GHSV of 19,800 NL kg_{cat}^{-1} h^{-1}, and a $CO_2/H_2/N_2$ = 3:9:2 feed gas. Based on these results, specific HPA loadings for alumina and zirconia were tested. From all bifunctional catalysts, a representative selection of favorable catalyst systems was used for extended measurements at 250 and 270 °C for 7 days each, keeping the other conditions constant. The GHSV used was selected in a regime, where thermodynamics and kinetics compete for reaction control and allow to differentiate between the performances of the catalyst systems tested.[48]

CtM Catalyst Preparation: CZZ. The CZZ catalyst for the CtM reaction was synthesized by co-precipitation from an aqueous metal nitrate solution (1 M, Cu:Zn:Zr 3.7:1.7:1 atom ratio) and Na_2CO_3 (1 M) as precipitating agents and then calcined (N_2 flow 5 NL h^{-1}; 200 °C h^{-1}; 300 °C for 2.5 h) to obtain the amorphous, black pre-catalyst. The yield of several syntheses (18 syntheses with each 5 g yield) was combined to form the large homogeneous batch used for this work. The pre-catalyst was *in situ* reduced in the reactor to form the actual catalyst (Figure 1, left). Synthesis details were published elsewhere.[48]

MtD Catalyst and Carrier Preparation: Zeolites, Alumina, Zirconia, and HPA Coating. Zeolites in their ammonia form ("NH_4^+") were calcined to obtain the Brønsted form ("H") and then further calcined to reduce the number of Brønsted acid sites and increase the number of Lewis acid sites ("L"). The β-zeolite (*CP814E*, SiO_2/Al_2O_3 mole ratio 25, SA_{BET} = 680 m^2/g, *Zeolyst International*) was calcined at 500 °C (600 °C h^{-1}) for 5 h (N_2 flow: 5.5 NL h^{-1}) to obtain "ZeoH". The ferrierite (*CP914C*, SiO_2/Al_2O_3 mole ratio 20, SA_{BET} = 400 m^2 g^{-1}, *Zeolyst International*) was calcined at 550 °C for 4 h under air flow to obtain "FERH".[30] These zeolites were further calcined two times at 750 °C (600 °C h^{-1}) for 5 h each (N_2 flow: 5.5 NL h^{-1}) to obtain "ZeoL" and "FERL". Alumina (γ-Al_2O_3, AlO_x) and zirconia (monoclinic, ZrO_2, ZrO_x) were provided by *Clariant GmbH* and used as received. HPA-coated AlO_x, FERH, FERL, ZeoH, ZeoL, and ZrO_x were synthesized by wet impregnation. Carrier and respective amount of heteropolyacid (tungstosilicic acid hydrate, "Si-HPA", >99.9%, *Sigma-Aldrich*, or phosphotungstic acid hydrate, "P-HPA", >99.995%, *Roth*) were mixed with ethanol and stirred at room temperature until dry (cf. SI-II.b). The coated dehydration catalysts are referred to as "HPA@Carrier xx", where "HPA" is either "Si-HPA" or "P-HPA". "@" indicates direct contact of coating and carrier. "xx" indicates the weight percentage of HPA compared to the carrier material. One must note that the chosen nomenclature is also common in the field of core−shell catalysts. The nomenclature was chosen to facilitate the reading and understanding of the catalyst compositions. We note that this is common praxis in this field of study.[40] A schematic overview of the synthesis of the MtD catalysts is given in Figure 1 (right).

Catalyst Testing. Experiments were performed on a four-channel parallel reactor test setup with online GC analysis (custom *GC8890*, *Agilent*).[48] The catalyst (100−200 mg, 100−200 μm) was mixed with silicon carbide (SiC, <210 μm, *VWR*) to a total mass of 1 g. The SiC-catalyst mixture was fixed between glass wool studs in a glass-walled steel reactor (ID 4 mm, *Trajan*). After an *in situ* reduction procedure with increasing H_2 content and pressure at 240 °C (for details, see elsewhere[48]), the reactors were purged with the feed gas mixture for 3 h. Measurements were performed consecutively at 250 °C (T_1), 230 °C (T_2), 210 °C (T_3), 270 °C (T_4), and 250 °C (T_5) with a GHSV of 19,800 NL kg_{cat}^{-1} h^{-1} (eq 1) of $CO_2/H_2/N_2$ 3:9:2 feed gas at 40 bar. Each temperature step was held for 8 h. The time on stream (ToS) between the first and last measurements for each catalyst system was 32 h. Due to the consecutive nature of the testing procedure, the first data point of each catalyst was measured between 0 h < ToS < 8 h. Detailed results are listed in Table 3. Extended measurements used the identical reduction procedure. The extended measurements were performed at 250 or 270 °C (Figure 9) with a GHSV of 19,800 NL kg_{cat}^{-1} h^{-1} with a feed gas composition of $CO_2/H_2/N_2$ 3:9:2 at a pressure of 40 bar. The ToS was set to 7 days (160 h).

Characterization Methods. All materials were analyzed by powder X-ray diffraction (pXRD; SI-II.d), thermogravimetric analysis (TGA; 10 °C min^{-1}, N_2 atmosphere; SI-II.f), differential scanning calorimetry (DSC; 10 °C min^{-1}, N_2 atmosphere; SI-II.f), Fourier transform infrared spectroscopy (FT-IR; SI-II.e), and N_2 physisorption (SA_{BET}, PV_{BJH}; pretreatment: high vacuum, 150 °C, 5 h). Atom absorption spectroscopy, temperature-programmed reduction, and N_2O reactive frontal chromatography were performed on the CZZ part, and exact method details were published elsewhere.[48,51] NH_3-TPD (10% NH_3 in He, He flow 20 mL min^{-1}, 10 °C min^{-1}, T_{max} = 600 °C) was performed on a carrier material. The measurements were performed with and without NH_3 loading to separate NH_3 from other desorption and decomposition products on the used thermal conductivity detector. Full details are published elsewhere.[48] SEM and EDX measurements were performed on the MtD catalyst materials Si-HPA@AlO_x 58 and Si-HPA@ZrO_x 31.

Definitions of Magnitudes Used.

$$\text{Gas hourly space velocity GHSV} = \frac{\dot{n}}{m_{CZZ}} = \left[\frac{\text{NL}}{kg_{CZZ}\cdot h}\right] \quad (1)$$

GHSV is the ratio of input gas flow ($\dot{n}$) and the amount of referenced catalyst (m_{CZZ}). For easier comparison with literature and for other researchers, we decided to use NL kg_{cat}^{-1} h^{-1} as the unit for the input gas flow and kg as the unit for the mass of the catalyst used.

$$CO_2 \text{ conversion } X_{CO_2} = \left(1 - \tilde{\varphi}_{N_2}\cdot\frac{\varphi_{CO_2,out}}{\varphi_{CO_2,in}}\right)\cdot 100\% = [\%] \quad (2)$$

Volume fraction of CO_2 measured from bypass as a measure for the CO_2 amount in the feed gas: $\varphi_{CO_2,in}$ = [Vol %].

https://doi.org/10.1021/acsomega.3c00149
ACS Omega 2023, 8, 15203−15216

Volume fraction of CO_2 measured from the reactor pass through: $\varphi_{CO_2,\,out}$ = [Vol %]. Volume contraction $\tilde{\varphi}_{N_2}$ as the ratio of amount $N_{2,out}$ and $N_{2,in}$.

$$\text{Selectivity, carbon based } S_i = 100\% \cdot \frac{a_i \varphi_i}{\sum_j a_j \varphi_j} = [\%] \quad (3)$$

Amount of substance i or j, with i/j being MeOH, DME, CO, or CH_4: φ_j = [Vol%]. Stoichiometric chemical reaction coefficient: a_j and a_j. Sum overall carbon-based products: $\sum_j a_j \varphi_j$ = [Vol%].

$$\text{Yield } Y_i = X_{CO_2} \cdot \frac{S_i}{100\%} = [\%] \quad (4)$$

Carbon-based amount of a molecule i (i = CO_2, CO, CH_4, MeOH, or DME) or a combination thereof, e.g., combined yield of all oxygenates Y_{Me} as the sum of Y_{DME} and Y_{MeOH}.

RESULTS AND DISCUSSION

First, the MeOH-producing, competitive CtM catalyst[48] is introduced, followed by a detailed analysis of all used MtD catalyst materials. The description of the underlying ideas for bifunctional catalyst preparation and nomenclature is followed by the results of the catalyst screening, which are sorted by the respective catalyst systems' ability to yield DME. From these findings, we delineate a close to ideal composition of the carrier material and HPA coating/preparation method for the most effective CtD. We end with insights on catalyst deactivation and extended measurements of a selection of catalysts.

Catalyst Properties. *CtM Catalyst.* Physical properties of the hydrogenation catalyst are measured for the pre-catalyst. *In situ*-activated CZZ and pre-catalyst are used synonymously. CZZ has an SA_{BET} of 110 $m^2\ g^{-1}$, a porous structure (PV_{BJH} = 0.394 $cm^3\ g^{-1}$), and a bulk density of 1030 mg cm^3 (100−200 μm). The FT-IR and pXRD results of the precursor and pre-catalyst were published elsewhere.[48]

Catalytic Activity of the CtM Catalyst. The results for catalytic activity of pure CZZ following the standard measurement procedure are shown in Figure 2 and Table 2.

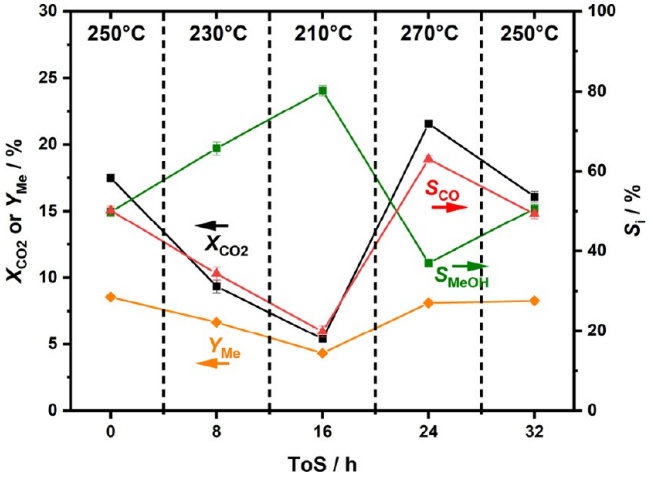

Figure 2. Results of pure CZZ following the standard measurement protocol of five consecutive temperature steps (T_1 = 250 °C, T_2 = 230 °C, T_3 = 210 °C, T_4 = 270 °C, and T_5 = 250 °C; cf. small graph) at 40 bar and GHSV 19,800 NL $kg_{cat}^{-1}\ h^{-1}$ with $CO_2/H_2/N_2$ 3:9:2.

Table 2. Results of Catalyst Testing for Pure CZZ[a]

T_x	X_{CO2}	Y_{Me}	S_{MeOH}	S_{CO}	ToS
°C	%	%	%	%	h
250 (T_1)	17.5 ± 0.3	8.6 ± 0.2	50 ± 1	50 ± 1	0
230 (T_2)	9.3 ± 0.5	6.7 ± 0.1	66 ± 2	34 ± 2	+8
210 (T_3)	5.4 ± 0.2	4.3 ± 0.1	80 ± 1	20 ± 1	+16
270 (T_4)	21.6 ± 0.2	8.1 ± 0.2	37 ± 1	63 ± 1	+24
250 (T_5)	16.1 ± 0.4	8.3 ± 0.1	51 ± 1	49 ± 1	+32

[a]Five consecutive temperature steps (T_1 = 250 °C, T_2 = 230 °C, T_3 = 210 °C, T_4 = 270 °C, and T_5 = 250 °C), each held for 8 h at 40 bar and GHSV 19,800 NL $kg_{cat}^{-1}\ h^{-1}$ with $CO_2/H_2/N_2$ 3:9:2. The error bars resemble the deviation of three separate measurements with four data points each.

At T_1, pure CZZ combines an X_{CO2} of 17.5% and an S_{MeOH} of 49.8% to a maximum in Y_{Me} (8.6%). Increasing the temperature to 270 °C (T_4) leads to higher X_{CO2} (21.6%) due to increased S_{CO} (63.0%) but slightly lower Y_{Me} (8.1%). Lower temperatures increase S_{MeOH} (65.7% (T_2) and 80.2% (T_3)) but decrease X_{CO2} (9.3% (T_2) and 5.4% (T_3)). The optimum operating temperature for the pure CZZ catalyst for the CtM reaction is 250 °C, as Y_{Me} is highest. Further, a loss in activity between T_1 and T_5 can be seen. The loss is more pronounced on X_{CO2} (−1.4%) than in Y_{DME} (−0.3%).

MtD Catalysts: Carrier Materials. Table 3 lists the SA_{BET}, pore volume, and HPA loading for all used MtD catalysts. Al_2O_3 (for better reading "AlO_x") and ZrO_2 (for better reading "ZrO_x") are Lewis acidic materials with a medium ($SA_{BET}(AlO_x)$ = 280 $m^2\ g^{-1}$) or small surface area ($SA_{BET}(ZrO_x)$ = 85 $m^2\ g^{-1}$). NH_3-TPD (Figure 3a,b) shows continuous NH_3 desorption from 100 to 300 °C. FERH (SA_{BET} = 407 $m^2\ g^{-1}$) and FERL (SA_{BET} = 467 $m^2\ g^{-1}$) represent the materials with medium−high surface areas, while ZeoH (SA_{BET} = 689 $m^2\ g^{-1}$) and ZeoL (SA_{BET} = 756 $m^2\ g^{-1}$) possess high surface areas. All zeolites show maximum NH_3 desorption (Figure 3c,d) below 300 °C but additional desorption above 300 °C. Overall, zeolites desorb more NH_3 than AlO_x and ZrO_x especially in the high-temperature region above 300 °C that are correlated with strong acid sites. FERL shows less NH_3 desorption than FERH, and the desorption curve shows a single peak around 150 °C. ZeoH and ZeoL show similar curves. Overall, the temperature treatment on the zeolites was found to have significantly changed the properties of FERL compared to FERH, while ZeoL shows miniscule changes compared to ZeoH. For a detailed discussion of the effect of the temperature treatment of the zeolites, see SI-III.

CtD Catalysts: HPA Coating and KU Loading. HPA was coated on carrier materials by wet impregnation. Weight ratios of carrier materials and Si-HPA of 2:1 (33 wt %), 1:1 (50 wt %), and 1:2 (67 wt %) were synthesized. AlO_x and ZrO_x were coated with P-HPA as well (carrier:P-HPA 1:1, 1:2). The carrier materials show high variance in their respective surface area ($SA_{BET}(ZeoL)$ = 756 $m^2\ g^{-1}$; $SA_{BET}(ZrO_x)$ = 85 $m^2\ g^{-1}$). KU loading per nm^2 of carrier material is a valuable addition for the discussion of the effect of HPA on the carrier material. The 67 wt % coatings of HPA result in KU loadings between 0.5 KU nm^{-2} (Si-HPA@ZeoL 67) and 4.7 KU nm^{-2} (Si-HPA@ZrO_x 67). The effect of HPA loading on physical properties can be seen in a decrease in SA_{BET} and pore volume (Table 3). The impact of HPA coating on the catalyst performance should be more pronounced on low surface carriers. pXRD and FT-IR show consecutive growth of HPA

https://doi.org/10.1021/acsomega.3c00149
ACS Omega 2023, 8, 15203−15216

Table 3. Summary of Specific Data and Catalysis Results of All Used Catalyst Systems[b]

name	HPA loading			SA_{BET}	PV_{BJH}	X_{CO2} (T_1)	X_{CO2} (T_5)	S_{DME} (T_1)	S_{DME} (T_5)
	carrier/HPA	wt %	KU nm^{-2}	$m^2\ g^{-1}$	$cm^3\ g^{-1}$	%	%	%	%
CZZ	-	-	-	110	0.394	17.5	16.1	49.8[a]	50.2[a]
Al	0.00	0	0.0	280	0.392	19.2(19.6)	18.2 (18.5)	0.3(0.4)	0.3(0.4)
Si-HPA@AlO_x 33	0.50	33	0.4	229	0.159	19.9(19.0)	18.3(17.7)	12.9(22.2)	9.3(20.6)
Si-HPA@AlO_x 50	1.00	50	0.7	151	0.060	17.3(−)	17.0(−)	26.1(−)	22.6(−)
Si-HPA@AlO_x 58	1.40	58	0.9	125	0.046	−(18.5)	−(16.8)	−(32.8)	−(32.8)
Si-HPA@AlO_x 67	2.00	67	1.4	104	0.030	18.5(17.7)	17.2(16.1)	32.1(33.1)	31.7(33.5)
Zr	0.00	0	0.0	85	0.320	20.0(20.0)	18.5(18.0)	0.0(0.1)	0.0(0.1)
Si-HPA@ZrO_x 31	0.45	31	1.1	94	0.176	−(17.9)	−(17.0)	−(33.8)	−(34.0)
Si-HPA@ZrO_x 33	0.50	33	1.2	93	0.141	18.7(19.2)	16.9(17.1)	33.3(33.3)	32.8(33.2)
Si-HPA@ZrO_x 50	1.00	50	2.3	86	0.075	13.3(−)	12.8(−)	34.1(−)	32.9(−)
Si-HPA@ZrO_x 67	2.00	67	4.7	68	0.035	18.6(−)	16.7(−)	28.9(−)	32.1(−)
P-HPA@AlO_x 50	1.00	50	0.7	151	0.063	20.2(−)	18.4(−)	3.0(−)	2.1(−)
P-HPA@AlO_x 67	2.00	67	1.4	97	0.046	18.4(−)	17.5(−)	4.6(−)	3.8(−)
P-HPA@ZrO_x 50	1.00	50	2.3	48	0.091	18.6(−)	17.7(−)	3.0(−)	1.0(−)
P-HPA@ZrO_x 67	2.00	67	4.7	29	0.050	19.8(−)	17.9(−)	14.8(−)	7.5(−)
FERH	0.00	0	0.0	407	0.038	13.6(18.3)	10.4(16.7)	3.5(32.3)	3.6(31.9)
Si-HPA@FERH 33	0.50	33	0.2	275	0.047	17.5(19.7)	14.1(17.7)	21.7(33.9)	15.4(33.5)
Si-HPA@FERH 50	1.00	50	0.5	238[a]	0.025[a]	15.0(−)	12.1(−)	32.8(−)	32.8(−)
Si-HPA@FERH 67	2.00	67	1.0	153	0.017	14.3(18.8)	12.9(16.6)	35.4(33.1)	36.6(33.0)
FERL	0.00	0	0.0	467	0.036	15.3(18.1)	12.0(15.3)	34.8(34.2)	36.5(35.1)
Si-HPA@FERL 33	0.50	33	0.2	320	0.026	18.7(18.9)	15.3(16.6)	33.6(33.8)	33.8(34.0)
Si-HPA@FERL 50	1.00	50	0.4	255	0.008	18.0(−)	14.7(−)	33.7(−)	34.2(−)
Si-HPA@FERL 67	2.00	67	0.9	181	0.026	17.4(−)	14.6(−)	33.1(−)	33.8(−)
ZeoH	0.00	0	0.0	689	0.615	12.6(18.6)	8.7(17.4)	35.6(33.0)	40.9(32.7)
Si-HPA@ZeoH 33	0.50	33	0.1	417[a]	0.234[a]	16.7(19.4)	11.9(17.2)	32.7(33.8)	34.6(33.6)
Si-HPA@ZeoH 50	1.00	50	0.3	388	0.183	16.1(−)	11.6(−)	33.4(−)	35.2(−)
Si-HPA@ZeoH 67	2.00	67	0.6	273[a]	0.124[a]	15.3(−)	12.3(−)	33.5(−)	35.3(−)
ZeoL	0.00	0	0.0	756	0.616	10.2(17.7)	6.8(16.7)	38.4(34.1)	43.4(33.9)
Si-HPA@ZeoL 33	0.50	33	0.1	345	0.288	17.1(19.5)	11.3(17.4)	32.7(33.5)	34.9(33.1)
Si-HPA@ZeoL 50	1.00	50	0.3	240	0.206	16.2(−)	11.6(−)	33.7(−)	35.5(−)
Si-HPA@ZeoL 67	2.00	67	0.5	312	0.115	16.6(−)	11.8(−)	32.6(−)	34.2(−)

[a]Pretreatment in vacuum at 200 °C, 5 h. [b]X_{CO2} and S_{DME} values for the first temperature step (T_1 = 250 C) and last temperature step (T_5 = 250 °C, ToS + 32 h). Values are from sole CZZ, homogeneous, and heterogeneous (parentheses) prepared bifunctional catalysts. Non-performed measurements are indicated with a "-".

signals with HPA mass (for details, see SI-II). Regarding the acid sites, one has to consider that replacement of a partially Brønsted or Lewis acidic material, e.g., zeolites, by a fully Brønsted acidic material increases the share of Brønsted acid sites of total acid sites, even though the total number of acid sites per mass or surface area might decrease. Following this argument, the share of Brønsted acid sites is assumed to increase with the weight percentage of HPA. As NH_3-TPD is unable to distinguish between different types of acid sites and specific sensor molecule IR techniques (e.g., pyridine-IR[52]) are unsuited for HPAs due to their decomposition under the needed conditions, no quantification and determination of the actual acid sites were performed.

CtD Catalysts: Synthesis and Nomenclature of Bifunctional Catalysts. The hydrogenation catalyst CZZ and the dehydration catalysts (MtD-Cat) were mixed in two ways (Figure 4): (i) "homogeneous" or (ii) "heterogeneous", as detailed in the experimental part. The homogeneous mixing method was a 1:1 weight ratio of CZZ and MtD-Cat thoroughly mixed in an agate mortar, then pressed, and sieved (100−200 μm). Homogeneously prepared catalysts are referred to as "CZZ + MtD-Cat". "+" emphasizes the intimate contact of both components. For the heterogeneous mixing method, CZZ and dehydration component were pressed and sieved (100−200 μm) separately and then physically mixed in a 1:1 weight ratio. Heterogeneously prepared catalysts are referred to as "CZZ//MtD-Cat". "//" symbolizes the missing direct contact of both components. All used catalyst components including HPA loading, SA_{BET}, and pore volume are listed in Table 3.

Catalyst Screening. The main factors for effective CO_2 valorization are the percentage of CO_2 converted in a single pass (X_{CO2}, eq 2) and the selectivity of the conversion toward the desired valuable product (S_i, eq 3), in this case DME (S_{DME}). The combination of conversion and selectivity results in the yield of a certain product (Y_i, eq 4). Therefore, Y_{DME} is the best suited measure for comparison of the MtD catalyst systems' performance. In addition, the combined yield of all oxygenates (Y_{Me}) is a good measure to compare overall CtD catalyst's effectiveness in CO_2 valorization. As the CtM component is the same for all catalyst systems, our main means of differentiation is Y_{DME}. All catalysis results shown in Figure 5a (T_1 = 250 °C, 40 bar, $CO_2/H_2/N_2$ 3:9:2, GHSV 19,800 NL $kg_{cat}^{-1}\ h^{-1}$) are sorted by Y_{DME} from low to high. X_{CO2} is shown as black dots, and S_i as bars. The measurement point with the highest Y_{Me} for the MeOH-producing CZZ part is 250 °C; hence, this temperature will be discussed in detail. Figure 5b shows the Y_{DME} for the temperature steps T_1 to T_4,

https://doi.org/10.1021/acsomega.3c00149
ACS Omega 2023, 8, 15203−15216

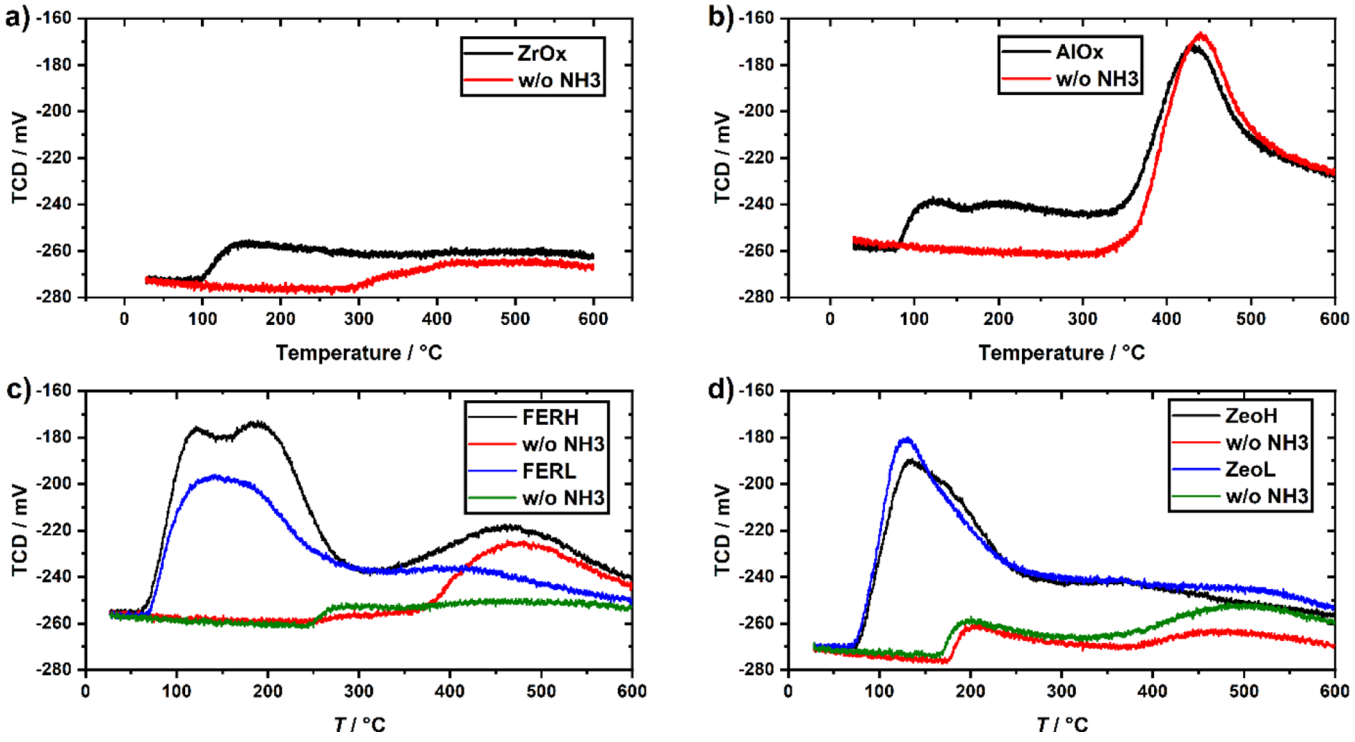

Figure 3. NH_3-TPD results of (a) AlO_x, (b) ZrO_x, (c) FERH and FERL, and (d) ZeoH and ZeoL. Measurements were performed twice, once with and on a new sample without NH_3 loading ("w/o NH3"). The area between both curves is the amount of desorbed NH_3.

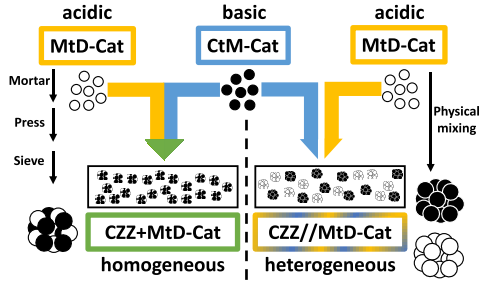

Figure 4. Synthesis scheme of the bifunctional catalysts (CtD catalysts). Homogeneous preparation leads to combined secondary particles or "single grain" bifunctional catalyst systems with high intraparticular interfaces and intensive contact between basic CtM and acidic MtD catalysts ("CZZ + MtD-cat"). Heterogeneous preparation leads to separate secondary particles or "dual grain" bifunctional catalysts with low contact due to separated basic and acidic particles ("CZZ//MtD-Cat").

while Figure 5c shows Y_{Me}. Figure 5d shows the difference between T_5 and T_1, to highlight changes happening over the course of the testing procedure. Detailed results of T_2 (230 °C), T_3 (210 °C), and T_4 (270 °C) are listed in Tables S3 to S6. The graphic is coarsely divided in three main regions: (left) low Y_{DME}, (middle) medium Y_{DME}, and (right) high Y_{DME}. On the low Y_{DME} side is the sole CtM catalyst (CZZ) with an X_{CO2} of 17.5%, an S_{MeOH} of 50%, and no S_{DME}. Next to it are the homogeneously and heterogeneously prepared bifunctional catalysts containing uncoated AlO_x and ZrO_x, followed by all tested P-HPA-coated catalyst systems. In the middle region, CZZ + Si-HPA@ZrO_x 67 stands out as it is the only catalyst system producing CH_4 in a parasitic side reaction. CZZ + Si-HPA@ZrO_x 67 is the catalyst system with the highest KU loading (4.7 KU nm^{-2}). The best suited catalyst systems accumulate in the right region of the figure and are mostly prepared heterogeneously. Thirteen out of the top 17 catalyst systems contain Si-HPA-coated MtD catalysts. Note that the conversions X_{CO2} found for CtD are far from the theoretical thermodynamic limit of 32% at 250 °C and 40 bar. A selection of catalysts from this catalyst screening was found to reach up to X_{CO2} = 30% at a lower GHSV of 1650 NL kg_{cat}^{-1} h^{-1} in our preceding thermodynamic investigation.[48]

Effect of Temperature on Bifunctional Catalyst Activity. Comparing the results of all temperatures measured, it becomes clear that X_{CO2} is no decisive factor, as S_{CO} increases with temperature and dominates the reaction network. For CO_2 valorization, the yield of oxygenates, like MeOH (Y_{MeOH}), DME (Y_{DME}), or their sum (Y_{Me}), is the relevant magnitude. The Y_{DME} for all high DME-producing bifunctional catalysts increases with temperature, reaching a maximum at 270 °C (Figure 5b, right section). The dependency of Y_{Me} on the temperature (Figure 5 c) underlines that active DME catalysts profit from a temperature increase in the overall higher Y_{DME} with higher temperatures, even though the pure CZZ catalyst shows a clear maximum in Y_{Me} at 250 °C (Figures 2 and 5c). Catalysts producing no or low amounts of DME reach a maximum of Y_{Me} at 250 °C, where they either level their activity or lower it (Figure 5b,c, left and middle section).

Effect of the Preparation Method on Catalyst Activity: Homogeneous vs Heterogeneous. For the further discussion of catalysts, a heat map plot, sorting the catalysts by the preparation method and HPA loading, gives a better overview. Figure 6 shows the X_{CO2} and S_{DME} for all homogeneously (Figure 6a,b) as well as heterogeneously prepared (Figure 6c,d) CtD catalyst systems. The heat map shows the used carrier MtD catalyst material (x-axis) with the corresponding amount of Si-HPA (y-axis). Phosphotungstic acid-coated catalyst systems are not further considered, as they

https://doi.org/10.1021/acsomega.3c00149
ACS Omega 2023, 8, 15203−15216

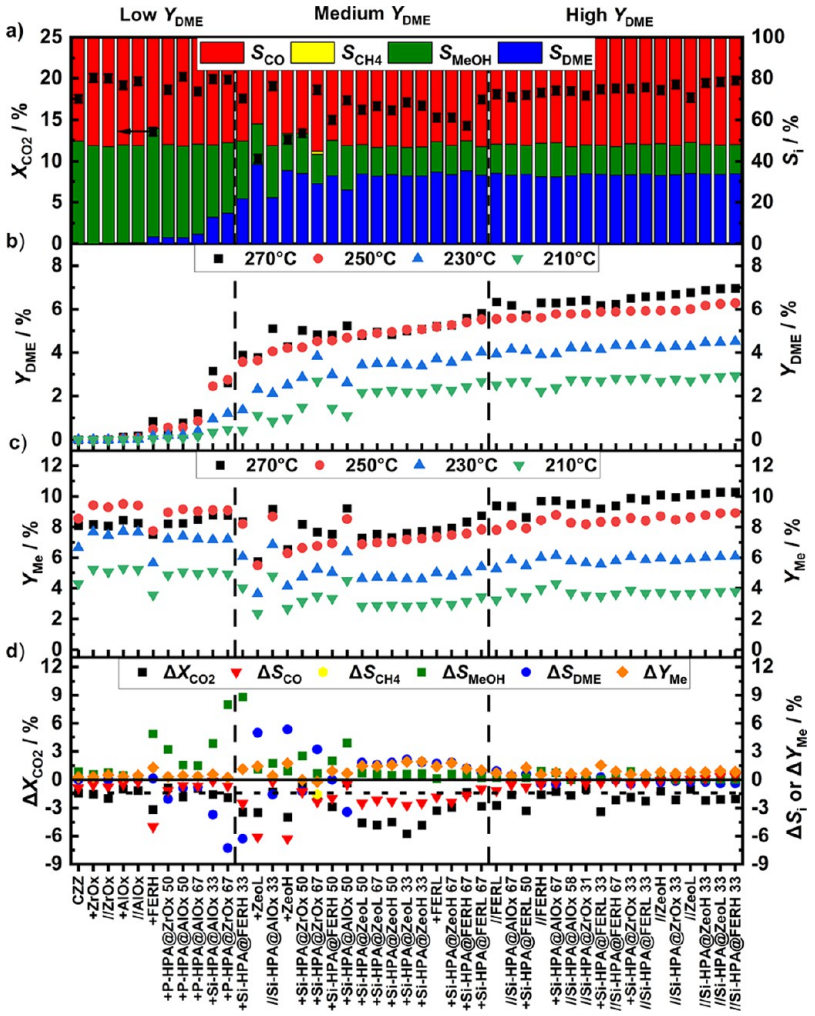

Figure 5. Results of all tested catalysts. (a) T_1 = 250 °C sorted by Y_{DME} from low to high. X_{CO2} is marked as squares including error bars (3 σ = 6%). Selectivity for all carbon-based products is shown as bar diagram: S_{CO} (red), S_{CH4} (yellow), S_{MeOH} (green), and S_{DME} (blue). Vertical dashed lines indicate the separation in the three main regions: (left) low Y_{DME}, (middle) medium Y_{DME}, and (right) high Y_{DME}. Results are from the first of five consecutive temperature steps T_1 = 250 °C at 40 bar, $CO_2/H_2/N_2$ 3:9:2, and GHSV 19,800 NL kg_{cat}^{-1} h^{-1}. (b) Results for Y_{DME} of T_1 (250 °C, red dots), T_2 (230 °C, blue triangle), T_3 (210 °C, green triangle), and T_4 (270 °C, black squares). (c) Results for Y_{Me} of T_1 (250 °C, red dots), T_2 (230 °C, blue triangle), T_3 (210 °C, green triangle), and T_4 (270 °C, black squares). (d) Difference of values of T_5 (250 °C) and T_1. ΔX_{CO2} (black squares), ΔS_{CO} (red triangles), ΔS_{CH4} (yellow hexagons), ΔS_{MeOH} (green squares), ΔS_{DME} (blue dots), and ΔY_{Me} (orange diamonds). For orientation, a line at zero and a dotted line at ΔX_{CO2}(CZZ) = −1.4% are added.

showed no relevant activity. The higher a value for X_{CO2} and S_{DME} is, the darker is its green color. Lower values are colored yellow to red.

Homogeneously Prepared/Single-Grain Bifunctional Catalysts: CZZ + MtD-Cat. CZZ + AlO_x and CZZ + ZrO_x show the highest values for X_{CO2} (+AlO_x, 19.2%, and +ZrO_x, 20.0%; Figure 6 a) but negligible S_{DME} values close to zero (Figure 6b). Uncoated AlO_x and ZrO_x are unsuited to produce DME under the chosen reaction conditions but enhance X_{CO2} compared to sole CZZ (17.5%). This might be due to water adsorption and the resulting interference in the reaction network. The CZZ + zeolites systems show values for X_{CO2} in the range of only $^2/_3$ (CZZ + FERL) to $^1/_2$ (CZZ + ZeoL) of that of CZZ + ZrO_x. CZZ + FERH shows comparably negligible low S_{DME} like CZZ + AlO_x and CZZ + ZrO_x. The rest of the tested zeolites show S_{DME} values between 35 and 38%. CZZ + FERH is impaired in the MeOH formation and inactive in the MtD reaction. The other zeolites show reduced MeOH formation abilities but are active in DME formation. After coating with Si-HPA, the prior non-DME active MtD catalyst AlO_x slightly decreases X_{CO2} with a Si-HPA loading of 50 wt %, but S_{DME} increases almost linearly with the amount of Si-HPA used (S_{DME} = 13 to 32%). CZZ + ZrO_x shows a significant decrease in X_{CO2} with a Si-HPA loading of 50 wt % and peaks in S_{DME} (33%) already at a Si-HPA coating of 33 wt %. All zeolite-containing catalysts reach a maximum of X_{CO2} with a Si-HPA loading of 33 wt %. FERH's S_{DME} profits from higher Si-HPA loadings, while the other zeolites show no effect on their S_{DME} with Si-HPA loading. In general, a Si-HPA coating increases X_{CO2} for lower CO_2-converting catalyst systems as well as it increases S_{DME} for lower DME-producing catalyst systems. Si-HPA coating seems to make homogeneously prepared single-grain bifunctional catalysts more resilient toward initial deactivation caused by the preparation method. The results indicate a specific most beneficial amount of Si-HPA for each MtD catalyst material.

Heterogeneously Prepared/Dual-Grain Bifunctional Catalysts: CZZ//MtD-Cat. From the results of the homoge-

https://doi.org/10.1021/acsomega.3c00149
ACS Omega 2023, 8, 15203−15216

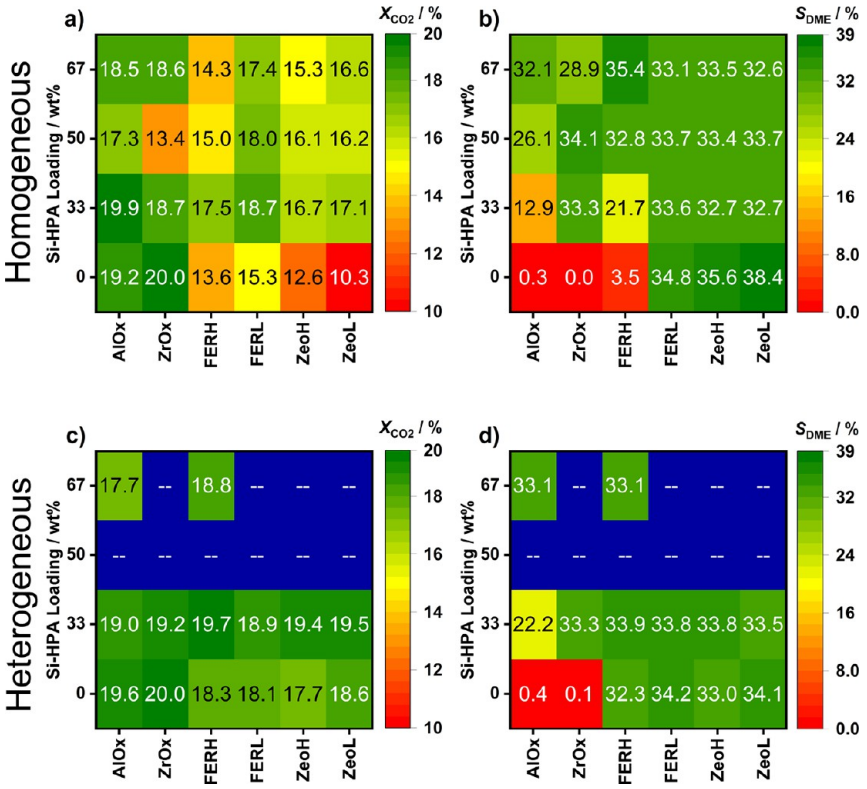

Figure 6. Heat map representation of catalysis results for X_{CO2} and S_{DME} at T_1 = 250 °C tested for homogeneously (a, b) and heterogeneously (c, d) prepared CtD catalysts. Values are colored as follows: high/good (green), middle/mediocre (yellow), and low/bad (red). Results are from the first of five consecutive temperature steps T_1 = 250 °C at 40 bar, $CO_2/H_2/N_2$ 3:9:2, and GHSV 19,800 NL kg_{cat}^{-1} h^{-1}. P-HPA catalysts are not shown due to lack of activity.

neously prepared bifunctional catalysts, a selection of catalysts was prepared heterogeneously. All uncoated MtD catalysts, all 33 wt % Si-HPA, and 67 wt % versions of AlO_x and FERH were tested heterogeneously prepared (CZZ//MtD-Cat). CZZ//AlO_x and CZZ//ZrO_x showed very close values for X_{CO2} (//AlO_x, 19.6%, and //ZrO_x, 20.0%) and negligible S_{DME} like their homogeneously prepared counterparts. All uncoated zeolite catalyst systems significantly increased their X_{CO2} to a similar level for all zeolites (18.2 ± 0.4%). The S_{DME} of CZZ//FERH matches the results of the other zeolite catalyst systems (33 ± 1%), now being a competitive MtD catalyst part. CZZ//Si-HPA@AlO_x 33 shows almost twice the S_{DME} (22%) as CZZ + Si-HPA@AlO_x 33 (13%) but peaks with CZZ//Si-HPA@AlO_x 67 at S_{DME} = 33%. The heterogeneously prepared CZZ//Si-HPA@ZrO_x 33 shows close to identical results as the homogeneously prepared counterpart CZZ + Si-HPA@ZrO_x 33. The Si-HPA-coated zeolite-containing catalysts slightly increase their X_{CO2}. The effect is especially pronounced for FERH-based bifunctional catalysts. CZZ//Si-HPA@FERH 33 shows an increase in X_{CO2} (19.7%, +2.2%) and S_{DME} (34%, +12%), while CZZ//Si-HPA@FERH 67 shows an increase in X_{CO2} (18.8%, +4.5%) compared to CZZ + Si-HPA@FERH 33 and CZZ + Si-HPA@FERH 67, respectively.

Overall, comparison of the preparation methods shows that the homogeneous method can induce initial deactivation of either one or both catalyst components. Under the chosen conditions, effective catalyst systems reach at least X_{CO2} values close to or above CZZ's values (X_{CO2} = 17.5%). S_{DME} ≈ 33% seems to be a limit for effective MtD catalysts under the chosen conditions. X_{CO2} < 17.5% is a sign for a partly deactivated CtM component, while S_{DME} < 33% indicates unsuited material properties or deactivation on the MtD component. Heterogeneous preparation seems to avoid initial deactivation through intimate contact, leading to increased X_{CO2} and/or S_{DME}. A detrimental effect caused by the distance between CZZ and MtD catalyst particles could not be seen. On the other hand, Si-HPA coating reduces the negative effects of homogeneous preparation and increases DME activity for all tested catalyst systems. P-HPA coatings show low DME activity and seem to be inferior to Si-HPA coatings. Si-HPA coatings increase Y_{DME} for all tested catalysts and increase the share of Brønsted acid sites in all acid sites. Y_{DME} shows to be independent from SA_{BET} (SI, Figure S26), further implying Brønsted sites to appear as superior acid sites for MeOH to DME conversion in a CO_2 feedstock. These results are in line with the findings of Navarro et al. using CZA with P-HPA@TiO_2 in the StD reaction.[39]

KU Loading of HPA and Preference for an Assumed Monolayer. Rojas et al.[33,34,53] tested various amounts of HPA coatings for the gaseous MtD conversion. They found the best KU loading to be 4.5 KU nm^{-2}, where each KU nm^{-2} indicates an assumed single layer of KU on the carrier's surface. Navarro et al.[38] tested P-HPA-coated TiO_2 with KU loadings of 1.4−2.7 KU nm^{-2} and a Cu/ZnO/Al_2O_3 catalyst in the direct CO to DME synthesis. In our screening, the only MtD catalyst reaching comparable KU loadings to Rojas et al. is Si-HPA@ZrO_x 67 with 4.7 KU nm^{-2}. Yet, CZZ + Si-HPA@ZrO_x 67 is the only CtD catalyst that produces the side product CH_4 in detectable quantities. As lower Si-HPA loadings did not produce detectable amounts of methane, the point can be made that ample abundance of Si-HPA enables methane production. However, Si-HPA-coated AlO_x catalysts suggest

https://doi.org/10.1021/acsomega.3c00149
ACS Omega 2023, 8, 15203−15216

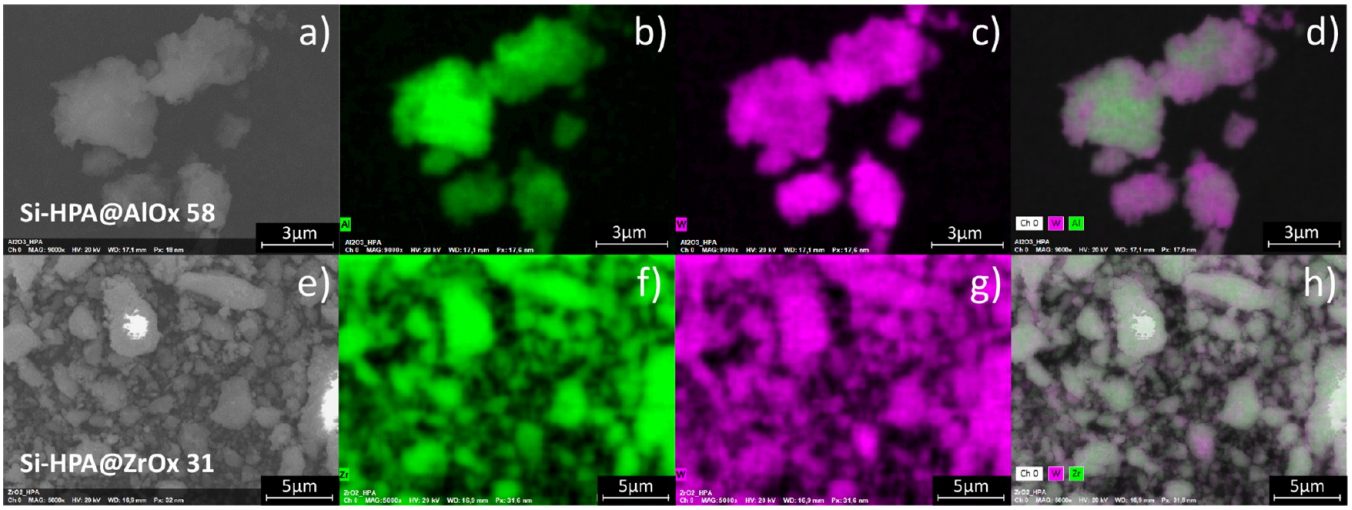

Figure 7. SEM and EDX analysis of Si-HPA@AlO_x 58 (a–d) and Si-HPA@ZrO_x 31 (e–h). Carrier material (AlO_x or Zr) is colored green, and tungsten (W) of Si-HPA is colored pink.

another reason: CZZ + Si-HPA@AlO_x 33 over CZZ + Si-HPA@AlO_x 50 to CZZ + Si-HPA@AlO_x 67 show an almost linear increase in S_{DME} with KU loadings of 0.4, 0.7, and 1.4 KU nm^{-2}, respectively. It appears that KU loadings around 1 KU nm^{-2} seem to be the most efficient for the CtD reaction and prevent overreactions, e.g., methane formation. Hence, a value of 1 KU nm^{-2} or an assumed monolayer of HPA on the carrier's surface should represent the best compromise between the surface area and acid site availability. From the heat map analysis, it is visible that especially DME inactive materials like AlO_x and ZrO_x benefit enormously from the Si-HPA coating. Therefore, Si-HPA loadings based on the surface area of AlO_x and ZrO_x, leading to 1 KU nm^{-2}, were synthesized and tested: Si-HPA@AlO_x 58 (58 wt % Si-HPA) and Si-HPA@ZrO_x 31 (31 wt % Si-HPA). Regarding the results in Figure 5a sorted by Y_{DME}, CZZ//Si-HPA@AlO_x 58 ranks as the most active Al-based CtD catalyst with an X_{CO2} of 18.5% and an S_{DME} of 33%, even though CZZ//Si-HPA@AlO_x 67 and CZZ + Si-HPA@AlO_x 67 are within the error range. CZZ//Si-HPA@ZrO_x 31 forms, within the error range of CZZ + Si-HPA@ZrO_x 33 and CZZ//Si-HPA@ZrO_x 33, the most active ZrO_x-based CtD catalyst. Si-HPA@AlO_x 58 and Si-HPA@ZrO_x 31 were investigated with SEM and EDX (Figure 7). The results show an even distribution of Si-HPA on the carrier's surface. Overall, too thick Si-HPA coatings cause side reactions to happen and loadings of 1 KU nm^{-2} seem to represent the best synergy of carrier's surface area and Si-HPA acid site availability for DME inactive carrier materials. Furthermore, wet impregnation can be stated as a suitable synthesis method.

Insights on Deactivation of CtD Catalysts. It is useful to divide the deactivation taking place into separate measurable scenarios. First, there is deactivation on the level of the preparation method or initial deactivation, visible in lower X_{CO2} values for a bifunctional catalyst than the pure CZZ system (cf. Figure 5a). Second, deactivation takes place over the course of the measurement protocol. Changes in catalyst activity can be related to different aspects of the bifunctional catalyst. A decrease in X_{CO2} but stable selectivities indicate a simultaneous deactivation occurring at all active sites. If a selectivity shift is observed, then the decrease in selectivity for the specific product is caused by deactivation of the specific active site, for which the selectivity decreased. An increase in selectivity due to an improvement of one type of an active site is unlikely; hence, the weight of argumentation will be laid on decreased selectivities. From these base-level considerations, the catalyst component or site of deactivation can be narrowed to the scenarios I to III:

I. Lower X_{CO2} (compared to pure CZZ), constant S_i: deactivation mainly occurs on the CtM component (CZZ).

II. Lower X_{CO2} (compared to pure CZZ), loss in S_{DME}: deactivation mainly occurs on the MtD component.

III. More pronounced decrease in X_{CO2} over time than pure CZZ: bifunctional character of the catalyst system accelerates deactivation.

In the literature, the main CtM deactivation reasons mentioned are temperature-controlled slow particle sintering. For MtD catalysts, "drowning" by water formation and coking are assigned.[24,54,55] In our work, the testing procedure consisted of five consecutive temperature steps (T_1 = 250 °C, T_2 = 230 °C, T_3 = 210 °C, T_4 = 270 °C, and T_5 = 250 °C) each held for 8 h; hence, the measurement at T_5 was taken 32 h after T_1. The test setup allows four catalysts to be tested simultaneously but measured consecutively. Hence, the first data point was captured between 0 h < ToS < 8 h, while the last point was captured 32 h later. The difference of the T_5 minus T_1 values represents the deactivation values ΔX_{CO2}, ΔS_i, and ΔY_{Me} given as absolute percentages (Figure 5d; cf. Table 3). In Figure 5d, a dashed horizontal line is added on the level of the measured deactivation for pure CZZ (ΔX_{CO2}(CZZ) = −1.4%). All bifunctional catalysts below this line show higher deactivation than pure CZZ, indicating that the MtD component interferes in the deactivation process. Sole CZZ shows a loss in an X_{CO2} of 1.4% (relative: −8%), with a small increase in S_{MeOH} of 1% (relative, +0.5%, ΔS_{CO} = −1%, relative, −0.5%). Hence, the sites for MeOH formation and RWGS are considered to deactivate equally. Most catalysts in the left (low Y_{DME}) and right (high Y_{DME}) regions show deactivation comparable to sole CZZ, indicating that the most relevant deactivation is due to processes happening on the CZZ catalyst independently from the MtD component. Some bifunctional catalysts in the middle region (medium Y_{DME})

https://doi.org/10.1021/acsomega.3c00149
ACS Omega 2023, 8, 15203−15216

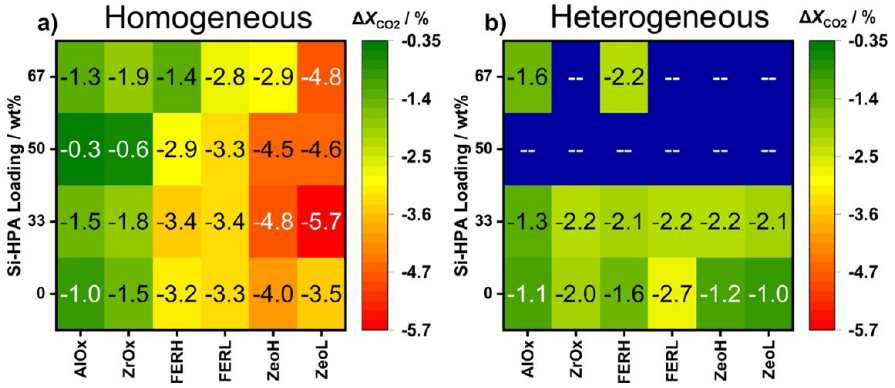

Figure 8. Absolute change in X_{CO2} visualized as a heat map for homogeneously (a) and heterogeneously (b) prepared bifunctional catalysts. The pure CZZ and less active P-HPA-containing catalysts are not shown. CZZ-level (ΔX_{CO2}: absolute = −1.4%; relative, −8%) deactivation is set to light green, less deactivated bifunctional catalysts are marked in dark green, and stronger deactivation is marked yellow to red.

show especially strong deactivation. Catalysts in the middle region showed to be DME active at T_1, with lower or comparable X_{CO2} than sole CZZ. A lower activity in the beginning (T_1; Figure 5 a) indicates deactivation caused by the preparation method. A more pronounced deactivation measured at the end (T_5) indicates inferior catalyst stability. One should note that all catalysts in the middle region that show a higher grade of deactivation were prepared by the homogeneous preparation method. Distinctive for this preparation method is the intimate contact of the surface-basic CtM and surface-acidic MtD component. During the homogeneous preparation, the basic and acidic surface properties of the catalyst components are brought to intimate contact. As the lower X_{CO2} is visible already at T_1, we assume a one-time event instead of a process to be its cause. A neutralization reaction between acid sites and basic ZnO on each material's surface would pose such an event. Hence, a surface-neutralization reaction between both materials induced through the intensive mixing in the agate mortar seems to be the main reason for deactivation. All systems sustained their yield of oxygenates or could increase it ($\Delta Y_{Me} \geq 0\%$), despite a loss in X_{CO2}. This agrees with the assignment that most deactivation happens on the active site for CO formation. The effect is most pronounced for homogeneously prepared catalyst systems in the medium Y_{DME} region. Heterogeneously prepared catalysts show overall less deactivation in X_{CO2} than their homogeneously prepared counterparts. Close to the same deactivation as pure CZZ are all heterogeneously prepared zeolite-based catalysts with 33 wt % Si-HPA, //FERH, //ZeoH, //ZeoL, //Si-HPA@ZrO_x 33, +Si-HPA@ZrO_x 33, and +Si-HPA@AlO_x 67 and the single-layered catalysts //Si-HPA@AlO_x 58 and //Si-HPA@ZrO_x 31. These bifunctional catalysts lead to the list of the most active DME yielding catalyst systems as well. This leads to the assumption that direct interaction between hydrogenation and dehydration components must be avoided to enable stability. Overly close proximity of the two catalyst functions is not necessary to form active catalyst systems.

Deactivation for uncoated and Si-HPA-coated catalysts is shown as a heat map in Figure 8 for easier comparison. Figure 8a shows all homogeneously prepared CtD catalysts, except CZZ and P-HPA-coated ones. Homogeneously prepared zeolite-based catalysts deactivate stronger than sole CZZ or AlO_x- and ZrO_x-based catalyst systems. On the other hand, all heterogeneously prepared CtD catalysts (Figure 8b) show similarly or slightly stronger deactivation than sole CZZ. This representation underlines the benefits of heterogeneous preparation on catalyst stability. Further, this leads to the finding that under the chosen conditions, all the active systems are comparable in activity and selectivity, if they are heterogeneously prepared. Further, the results imply that heterogeneously prepared bifunctional catalysts share a common deactivation mechanism, possibly caused by the increased amount of produced water due to MeOH dehydration in CtD compared to CtM.

Extended ToS: Stability at 250 and 270 °C. The activity limit of the CtM catalyst was found to be 250 °C, yet active CtD catalysts show a benefit from further elevated temperatures. A measurement period of 32 h is too short for extended stability estimation, and rapid fluctuation of temperature is uncommon in industrial processes. Therefore, longer measurement periods of 7 days (ToS = 160 h) were performed at 250 and 270 °C (40 bar, $CO_2/H_2/N_2$ 3:9:2, GHSV 19,800 NL kg_{cat}^{-1} h^{-1}). Ren et al. found a stronger deactivation over the course of 100 h ToS.[42] Bonura et al. found 260 °C at 30 bar with a GHSV of 8800 NL kg_{cat}^{-1} h^{-1} to be accelerating catalyst deactivation.[56] For extended measurements at 250 °C, pure CZZ, CZZ//FERH, CZZ//Si-HPA@AlO_x 58, and CZZ//Si-HPA@ZrO_x 31 were tested. The bifunctional catalysts were additionally tested at 270 °C to see if elevated temperatures yield higher amounts of DME on the cost of catalyst stability. The results are shown in Figure 9a−d (250 °C) and e−g (270 °C). All catalysts show high levels of stability at 250 and 270 °C. During the extended measurement period of 7 days, no drop in activity could be detected. X_{CO2} and Y_{Me} are decreasing for all catalyst materials, with a steeper decrease during the first 24 h, and then leveling out. At 250 °C, selectivities stay almost constant, while at 270 °C, an increase in S_{CO} can be seen.

For Y_{Me}, a decaying exponential function was fitted and high R^2 values were reached for all catalyst systems and temperatures (Table 4; for the graphical fit, cf. Figure S27). The function runs into an asymptotic value, which represents the stable value at which the catalyst system is expected to perform over a long period of time. At 250 °C, the pure CZZ reaches the expected stable limit after 78 h. The estimated asymptotic values for the bifunctional catalysts are lower than for pure CZZ; hence, they need longer ToS to reach the expected stable value. The lower expected values compared to CZZ indicate that the CtD reaction is more demanding on catalyst stability than CtM. The asymptotic value at 270 °C for all bifunctional

https://doi.org/10.1021/acsomega.3c00149
ACS Omega 2023, 8, 15203−15216

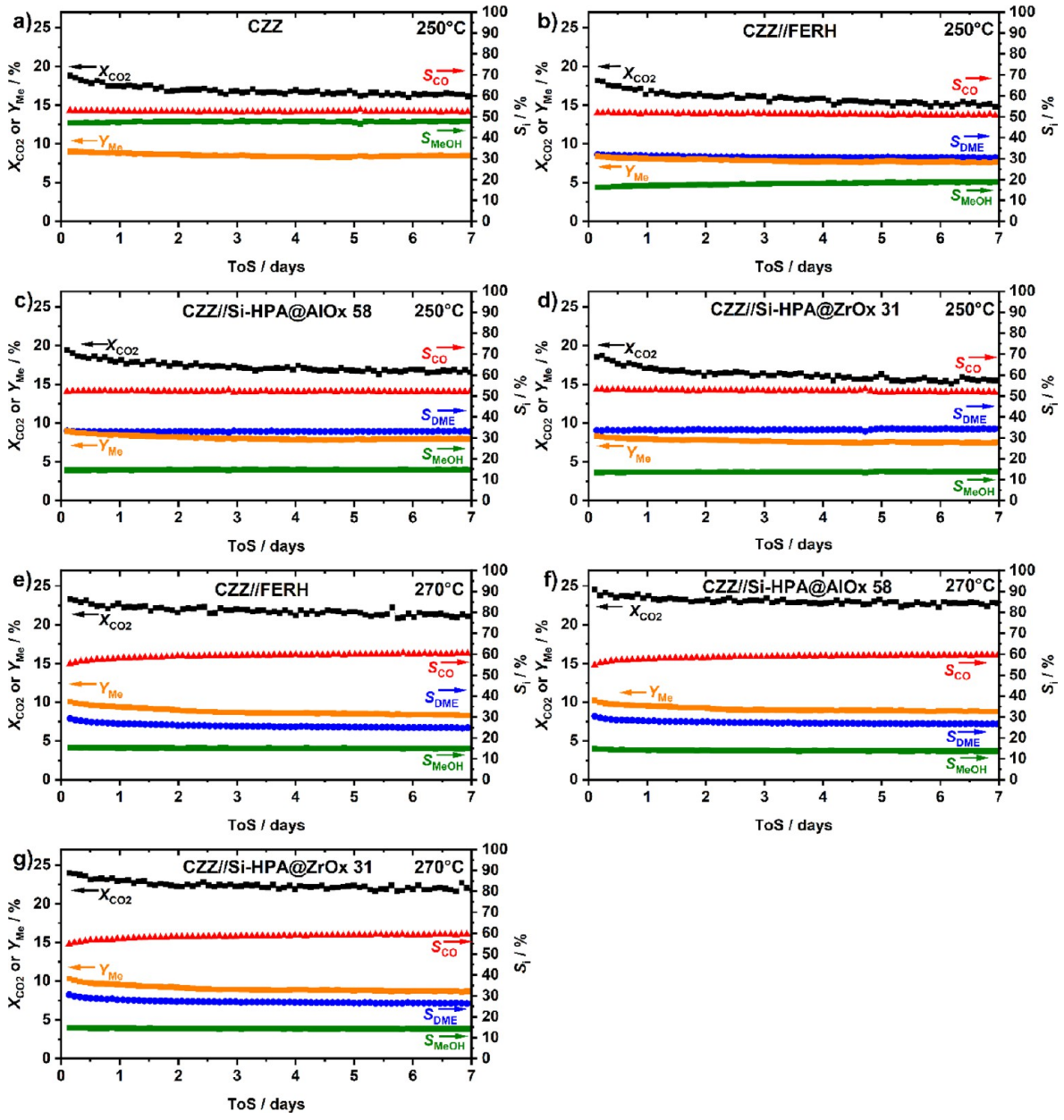

Figure 9. Extended measurement of 7 days (160 h), 40 bar, GHSV 19800 NL kg_{cat}^{-1} h^{-1}. Shown are X_{CO2} (black squares), S_{DME} (blue dots), S_{MeOH} (green squares), and S_{CO} (red triangles) of (a) CZZ (250 °C), (b) CZZ//FERH (250 °C), (c) CZZ//Si-HPA@AlO_x 58 (250 °C), (d) CZZ//Si-HPA@ZrO_x 31 (250 °C), (e) CZZ//FERH (270 °C), (f) CZZ//Si-HPA@AlO_x 58 (270 °C), and (g) CZZ//Si-HPA@ZrO_x 31 (270 °C).

catalysts lies above the expected value at 250 °C. Hence, elevated temperatures seem to represent the most effective operating window for bifunctional catalysts in the CtD reaction. It has to be noted that trustworthy estimation of catalyst lifetime or deactivation rates needs significantly longer ToS.

In conclusion, the selection of catalyst systems taken from the screening shows good stability in extended measurements. Within the error range, HPA-coated catalysts perform equally good, if not slightly better than the well-known FERH catalyst. Thus, Si-HPA-coated catalysts can be successfully added to the CtD catalyst toolbox. Higher activity in CO_2 valorization at elevated temperatures does not seem to affect catalyst stability under the chosen conditions. The high stability at constant temperatures indicates that varying conditions are more damaging to the catalyst activity than elevated temperatures. This leads to the assumption that the lower water desorption ability at lower temperatures is more demanding on catalyst stability than deactivation due to particle sintering.

CONCLUSIONS

A wide catalyst screening for the direct synthesis of DME with a CO_2/H_2 (1:3) feed gas was performed. Zeolites (ferrierites and β-zeolites), γ-Al_2O_3, ZrO_2, and HPA-coated versions thereof were mixed with Cu/ZnO/ZrO_2 catalysts. Two different mixing methods were tested. The intense single-grain method resulted in high initial catalyst deactivation, while the dual-grain method yielded overall more active bifunctional catalysts. HPA coatings with silicotungstic acid improved the resilience toward preparation-induced deactivation. Phosphotungstic acid, however, showed no relevant activity. Analysis of the KU loading showed assumed monolayers of Keggin units

https://doi.org/10.1021/acsomega.3c00149
ACS Omega 2023, 8, 15203−15216

Table 4. Results of Fitting a Decaying Exponential Function over the Extended Measurement Results[b]

catalyst	R^2	A %	B %	C %	ToS h
250 °C					
CZZ	0.90	0.78 ± 0.04	1.5 ± 0.1	8.37 ± 0.01	78
CZZ//FERH	0.94	0.79 ± 0.02	2.3 ± 0.2	7.59 ± 0.02	153
CZZ//Si-HPA@ AlO_x 58	0.97	1.14 ± 0.03	1.38 ± 0.07	7.86 ± 0.01	93
CZZ//Si-HPA@ ZrO_x 31	0.95	0.85 ± 0.02	2.2 ± 0.2	7.40 ± 0.01	160[a]
270 °C					
CZZ//FERH	0.99	1.76 ± 0.02	1.97 ± 0.07	8.32 ± 0.02	160[a]
CZZ//Si-HPA@ AlO_x 58	0.98	1.31 ± 0.02	1.56 ± 0.06	8.82 ± 0.01	139
CZZ//Si-HPA@ ZrO_x 31	0.98	1.58 ± 0.02	1.57 ± 0.06	8.69 ± 0.01	135

[a]The catalyst has not yet reached the respective asymptotic value. [b]The fit was performed using OriginPro 2021 by OriginLab Corporation. As fitting function "ExpDec1" was used. Equation: $y = A \cdot \exp(-x \cdot B^{-1}) + C$. C resembles the asymptotic values to which the function strives. Plots including the fit are shown in SI-VI.

to yield the most active catalysts for low SA_{BET} materials, even outperforming zeolites with four times higher SA_{BET}, showing no direct link of the surface area and activity. Further, a high share in Brønsted acid sites can be stated as preferred for MeOH dehydration in direct DME synthesis starting from CO_2. The combination of HPA coating and dual-grain preparation resulted in active and long-time stable bifunctional catalysts, even under challenging conditions. Comparison of the standard five-temperature-step procedure and stable extended procedure showed that fluctuating temperatures are more demanding on the catalyst activity than higher but stable temperatures.

■ ASSOCIATED CONTENT

Supporting Information

The Supporting Information is available free of charge at https://pubs.acs.org/doi/10.1021/acsomega.3c00149.

Catalyst synthesis details, material characterization (pXRD, FT-IR, TGA, DSC), further discussion on the effect of temperature treatment on commercial zeolites, catalyst activity comparison of the base of SA_{BET} and Y_{DME}, catalysis results of the temperature steps T_2 = 230 °C, T_3 = 230 °C, and T_4 = 270 °C, and extended measurement results including calculated fit (PDF)

■ AUTHOR INFORMATION

Corresponding Author

Ingo Krossing − *Institut für Anorganische und Analytische Chemie, Universität Freiburg, 79104 Freiburg, Germany; Freiburger Materialforschungszentrum (FMF), Universität Freiburg, 79104 Freiburg, Germany;* orcid.org/0000-0002-7182-4387; Email: krossing@uni-freiburg.de

Authors

Dustin Kubas − *Institut für Anorganische und Analytische Chemie, Universität Freiburg, 79104 Freiburg, Germany; Freiburger Materialforschungszentrum (FMF), Universität Freiburg, 79104 Freiburg, Germany;* orcid.org/0000-0002-1683-5470

Jennifer Maria Beck − *Institut für Anorganische und Analytische Chemie, Universität Freiburg, 79104 Freiburg, Germany; Freiburger Materialforschungszentrum (FMF), Universität Freiburg, 79104 Freiburg, Germany*

Erdogan Kasisari − *Institut für Anorganische und Analytische Chemie, Universität Freiburg, 79104 Freiburg, Germany*

Timo Schätzler − *Institut für Anorganische und Analytische Chemie, Universität Freiburg, 79104 Freiburg, Germany*

Anita Becherer − *Institut für Anorganische und Analytische Chemie, Universität Freiburg, 79104 Freiburg, Germany*

Anna Fischer − *Institut für Anorganische und Analytische Chemie, Universität Freiburg, 79104 Freiburg, Germany; Freiburger Materialforschungszentrum (FMF), Universität Freiburg, 79104 Freiburg, Germany;* orcid.org/0000-0003-4567-3009

Complete contact information is available at: https://pubs.acs.org/10.1021/acsomega.3c00149

Notes

The authors declare no competing financial interest.

■ ACKNOWLEDGMENTS

This work was supported by the Freiburg Material Research Center of the Albert-Ludwigs-Universität Freiburg and by the German Federal Ministry of Education and Research (BMBF) in the project *NAMOSYN* (03SF0566B0) for founding our research and the project EDELKAT (03X5524) for founding of the electron microscope. We would like to thank Prof. Dr. Jörg Sauer and Dr. Stephan Pitter from Karlsruhe Institute of Technology's (KIT) Institute of Catalysis Research and Technology (IKFT) for providing the FER material. We thank Dr. Andreas Geisbauer from Clariant GmbH for providing the Al_2O_3 and ZrO_2 material. From the Freiburg Material Research Center of the Albert-Ludwigs-Universität Freiburg, we thank Lukas Dietmar Ernst for pXRD measurements and Andreas Warmbold with Sultan D'Anucci for measurement of TGA, DSC, and BET.

■ REFERENCES

(1) Goeppert, A.; Czaun, M.; Jones, J.-P.; Prakash, G. K. S.; Olah, G. A. Recycling of carbon dioxide to methanol and derived products − closing the loop. *Chem. Soc. Rev.* **2014**, *43*, 7995−8048.

(2) Schlögl, R. *Chemical Energy Storage*; de Gruyter: Berlin, 2013, DOI: 10.1515/9783110266320.

(3) Styring, P.; Dowson, G. R. M.; Tozer, I. O. Synthetic Fuels Based on Dimethyl Ether as a Future Non-Fossil Fuel for Road Transport From Sustainable Feedstocks. *Front. Energy Res.* **2021**, *9*, No. 663331.

(4) Wang, Y.; Liu, H.; Huang, Z.; Liu, Z. Study on combustion and emission of a dimethyl ether-diesel dual-fuel premixed charge compression ignition combustion engine with LPG (liquefied petroleum gas) as ignition inhibitor. *Energy* **2016**, *96*, 278−285.

(5) Drexler, M.; Haltenort, P.; Arnold, U.; Sauer, J. Continuous Synthesis of Oxymethylene Ether Fuels from Dimethyl Ether in a Heterogeneously Catalyzed Liquid Phase Process. *Chem. Ing. Tech.* **2022**, *94*, 256−266.

(6) Song, Q.-W.; Zhou, Z.-H.; He, L.-N. Efficient, selective and sustainable catalysis of carbon dioxide. *Green Chem.* **2017**, *19*, 3707−3728.

(7) Liu, Q.; Wu, L.; Jackstell, R.; Beller, M. Using carbon dioxide as a building block in organic synthesis. *Nat. Commun.* **2015**, *6*, 5933.

(8) Ribeiro, A. P. C.; Martins, L. M. D. R. S.; Pombeiro, A. J. L. Carbon dioxide-to-methanol single-pot conversion using a C-scorpionate iron(II) catalyst. *Green Chem.* **2017**, *19*, 4811−4815.
(9) Bukhtiyarova, M.; Lunkenbein, T.; Kähler, K.; Schlögl, R. Methanol Synthesis from Industrial CO_2 Sources: A Contribution to Chemical Energy Conversion. *Catal. Lett.* **2017**, *147*, 416−427.
(10) The Royal Society, Ed.; *Sustainable synthetic carbon based fuels: Policy Briefing*; The Royal Society, 46, 2019.
(11) Sun, J.; Yang, G.; Yoneyama, Y.; Tsubaki, N. Catalysis Chemistry of Dimethyl Ether Synthesis. *ACS Catal.* **2014**, *4*, 3346−3356.
(12) Frusteri, F.; Cordaro, M.; Cannilla, C.; Bonura, G. Multifunctionality of Cu-ZnO-ZrO_2/H-ZSM5 catalysts for the one-step CO_2-to-DME hydrogenation reaction. *Appl. Catal., B* **2015**, *162*, 57−65.
(13) Bonura, G.; Cannilla, C.; Frusteri, L.; Mezzapica, A.; Frusteri, F. DME production by CO_2 hydrogenation: Key factors affecting the behaviour of CuZnZr/ferrierite catalysts. *Catal. Today* **2017**, *281*, 337−344.
(14) Aguayo, A. T.; Ereña, J.; Mier, D.; Arandes, J. M.; Olazar, M.; Bilbao, J. Kinetic Modeling of Dimethyl Ether Synthesis in a Single Step on a CuO−ZnO−Al_2O_3/γ-Al_2O_3 Catalyst. *Ind. Eng. Chem. Res.* **2007**, *46*, 5522−5530.
(15) Álvarez, A.; Bansode, A.; Urakawa, A.; Bavykina, A. V.; Wezendonk, T. A.; Makkee, M.; Gascon, J.; Kapteijn, F. Challenges in the greener Production of Formates/Formic Acid, Methanol, and DME by heterogeneously Catalyzed CO_2 Hydrogenation Process. *Chem. Rev.* **2017**, *117*, 9804−9838. Published Online: Jun. 28, 2017.
(16) Stangeland, K.; Li, H.; Yu, Z. Thermodynamic Analysis of Chemical and Phase Equilibria in CO_2 Hydrogenation to Methanol, Dimethyl Ether, and Higher Alcohols. *Ind. Eng. Chem. Res.* **2018**, *57*, 4081−4094.
(17) Polierer, S.; Guse, D.; Wild, S.; Herrera Delgado, K.; Otto, T. N.; Zevaco, T. A.; Kind, M.; Sauer, J.; Studt, F.; Pitter, S. Enhanced Direct Dimethyl Ether Synthesis from CO_2-Rich Syngas with Cu/ZnO/ZrO_2 Catalysts Prepared by Continuous Co-Precipitation. *Catalysts* **2020**, *10*, 816.
(18) Arena, F.; Barbera, K.; Italiano, G.; Bonura, G.; Spadaro, L.; Frusteri, F. Synthesis, characterization and activity pattern of Cu−ZnO/ZrO_2 catalysts in the hydrogenation of carbon dioxide to methanol. *J. Catal.* **2007**, *249*, 185−194.
(19) Bonura, G.; Cannilla, C.; Frusteri, L.; Frusteri, F. The influence of different promoter oxides on the functionality of hybrid CuZn-ferrierite systems for the production of DME from CO_2 -H_2 mixtures. *Appl. Catal., A* **2017**, *544*, 21−29.
(20) Arena, F.; Mezzatesta, G.; Zafarana, G.; Trunfio, G.; Frusteri, F.; Spadaro, L. How oxide carriers control the catalytic functionality of the Cu−ZnO system in the hydrogenation of CO_2 to methanol. *Catal. Today* **2013**, *210*, 39−46.
(21) Arena, F.; Mezzatesta, G.; Zafarana, G.; Trunfio, G.; Frusteri, F.; Spadaro, L. Effects of oxide carriers on surface functionality and process performance of the Cu−ZnO system in the synthesis of methanol via CO_2 hydrogenation. *J. Catal.* **2013**, *300*, 141−151.
(22) Dadgar, F.; Myrstad, R.; Pfeifer, P.; Holmen, A.; Venvik, H. J. Direct dimethyl ether synthesis from synthesis gas:The influence of methanol dehydration on methanol synthesis reaction. *Catal. Today* **2016**, *270*, 76−84.
(23) Dadgar, F.; Myrstad, R.; Pfeifer, P.; Holmen, A.; Venvik, H. J. Catalyst Deactivation During One-Step Dimethyl Ether Synthesis from Synthesis Gas. *Catal. Lett.* **2017**, *147*, 865−879.
(24) Sobczak, J.; Wysocka, I.; Murgrabia, S.; Rogala, A. A Review on Deactivation and Regeneration of Catalysts for Dimethyl Ether Synthesis. *Energies* **2022**, *15*, 5420.
(25) Huber, P.; Studt, F.; Plessow, P. N. Reactivity of Surface Lewis and Brønsted Acid Sites in Zeolite Catalysis: A Computational Case Study of DME Synthesis Using H-SSZ-13. *J. Phys. Chem. C* **2022**, *126*, 5896−5905.
(26) Palomo, J.; Rodríguez-Cano, M. Á.; Rodríguez-Mirasol, J.; Cordero, T. ZSM-5-decorated CuO/ZnO/ZrO_2 fibers as efficient bifunctional catalysts for the direct synthesis of DME from syngas. *Appl. Catal., B* **2020**, *270*, No. 118893.
(27) Bonura, G.; Frusteri, F.; Cannilla, C.; Drago Ferrante, G.; Aloise, A.; Catizzone, E.; Migliori, M.; Giordano, G. Catalytic features of CuZnZr−zeolite hybrid systems for the direct CO_2-to-DME hydrogenation reaction. *Catal. Today* **2016**, *277*, 48−54.
(28) Catizzone, E.; Aloise, A.; Giglio, E.; Ferrarelli, G.; Bianco, M.; Migliori, M.; Giordano, G. MFI vs. FER zeolite during methanol dehydration to dimethyl ether: The crystal size plays a key role. *Catal. Commun.* **2021**, *149*, No. 106214.
(29) Migliori, M.; Condello, A.; Dalena, F.; Catizzone, E.; Giordano, G. CuZnZr-Zeolite Hybrid Grains for DME Synthesis: New Evidence on the Role of Metal-Acidic Features on the Methanol Conversion Step. *Catalysts* **2020**, *10*, 671.
(30) Wild, S.; de Oliveira Campos, B. L.; Zevaco, T. A.; Guse, D.; Kind, M.; Pitter, S.; Delgado, K. H.; Sauer, J. Experimental investigations and model-based optimization of CZZ/H-FER 20 bed composition for the direct synthesis of DME from CO_2 -rich syngas. *React. Chem. Eng.* **2022**, 943−956.
(31) Schnee, J.; Eggermont, A.; Gaigneaux, E. M. Boron Nitride:A Support for Highly Active Heteropolyacids in the Methanol-to-DME Reaction. *ACS Catal.* **2017**, *7*, 4011−4017.
(32) Schnee, J.; Fusaro, L.; Aprile, C.; Gaigneaux, E. M. Keggin $H_3PW_{12}O_{40}$ pore blockage by coke can be reversible in the gas phase methanol-to-DME reaction. *Catal. Sci. Technol.* **2017**, *7*, 6151−6160.
(33) Ladera, R. M.; Ojeda, M.; Fierro, J. L. G.; Rojas, S. TiO_2 -supported heteropoly acid catalysts for dehydration of methanol to dimethyl ether: relevance of dispersion and support interaction. *Catal. Sci. Technol.* **2015**, *5*, 484−491.
(34) Peinado, C.; Liuzzi, D.; Ladera-Gallardo, R. M.; Retuerto, M.; Ojeda, M.; Peña, M. A.; Rojas, S. Effects of support and reaction pressure for the synthesis of dimethyl ether over heteropolyacid catalysts. *Sci. Rep.* **2020**, *10*, 8551. Published Online: May. 22, 2020.
(35) Liuzzi, D.; Peinado, C.; Peña, M. A.; van Kampen, J.; Boon, J.; Rojas, S. Increasing dimethyl ether production from biomass-derived syngas via sorption enhanced dimethyl ether synthesis. *Sustainable Energy Fuels* **2020**, *4*, 5674−5681.
(36) Kornas, A.; Śliwa, M.; Ruggiero-Mikołajczyk, M.; Samson, K.; Podobiński, J.; Karcz, R.; Duraczyńska, D.; Rutkowska-Zbik, D.; Grabowski, R. Direct hydrogenation of CO2 to dimethyl ether (DME) over hybrid catalysts containing CuO/ZrO2 as a metallic function and heteropolyacids as an acidic function. *React. Kinet., Mech. Catal.* **2020**, *130*, 179−194.
(37) Alharbi, W.; Kozhevnikova, E. F.; Kozhevnikov, I. V. Dehydration of Methanol to Dimethyl Ether over Heteropoly Acid Catalysts: The Relationship between Reaction Rate and Catalyst Acid Strength. *ACS Catal.* **2015**, *5*, 7186−7193.
(38) Millán, E.; Mota, N.; Guil-López, R.; Pawelec, B.; García Fierro, J. L.; Navarro, R. M. Direct Synthesis of Dimethyl Ether from Syngas on Bifunctional Hybrid Catalysts Based on Supported $H_3PW_{12}O_{40}$ and Cu-ZnO(Al): Effect of Heteropolyacid Loading on Hybrid Structure and Catalytic Activity. *Catalysts* **2020**, *10*, 1071.
(39) Millán Ordóñez, E.; Mota, N.; Guil-López, R.; Garcia Pawelec, B.; Fierro, J. L. G.; Navarro Yerga, R. M. Direct Synthesis of Dimethyl Ether on Bifunctional Catalysts Based on Cu−ZnO(Al) and Supported $H_3PW_{12}O_{40}$: Effect of Physical Mixing on Bifunctional Interactions and Activity. *Ind. Eng. Chem. Res.* **2021**, *60*, 18853−18869.
(40) Karaman, B. P.; Oktar, N.; Doğu, G.; Dogu, T. Heteropolyacid Incorporated Bifunctional Core-Shell Catalysts for Dimethyl Ether Synthesis from Carbon Dioxide/Syngas. *Catalysts* **2022**, *12*, 1102.
(41) Mondal, U.; Yadav, G. D. Direct synthesis of dimethyl ether from CO_2 hydrogenation over highly active, selective and stable catalyst containing Cu-ZnO-Al_2O_3/Al-Zr(1:1)-SBA-15. *React. Chem. Eng.* **2022**, 1391−1408.
(42) Ren, S.; Li, S.; Klinghoffer, N.; Yu, M.; Liang, X. Effects of mixing methods of bifunctional catalysts on catalyst stability of DME synthesis via CO_2 hydrogenation. *Carbon Resour. Convers.* **2019**, *2*, 85−94.

https://doi.org/10.1021/acsomega.3c00149
ACS Omega 2023, 8, 15203−15216

(43) Bae, J.-W.; Potdar, H. S.; Kang, S.-H.; Jun, K.-W. Coproduction of Methanol and Dimethyl Ether from Biomass-Derived Syngas on a Cu−ZnO−Al_2O_3/γ-Al_2O_3 Hybrid Catalyst. *Energy Fuels* **2008**, *22*, 223−230.
(44) Frusteri, L.; Bonura, G.; Cannilla, C.; Todaro, S.; Giordano, G.; Migliori, M.; Frusteri, F. Promoting Direct CO_2 Conversion to DME over Zeolite-based Hybrid Catalysts. *Pet. Chem.* **2020**, *60*, 508−515.
(45) Frusteri, F.; Migliori, M.; Cannilla, C.; Frusteri, L.; Catizzone, E.; Aloise, A.; Giordano, G.; Bonura, G. Direct CO_2 -to-DME hydrogenation reaction:New evidences of a superior behaviour of FER-based hybrid systems to obtain high DME yield. *J. CO2 Util.* **2017**, *18*, 353−361.
(46) Bizon, K.; Skrzypek-Markiewicz, K.; Continillo, G. Enhancement of the Direct Synthesis of Dimethyl Ether (DME) from Synthesis Gas by Macro- and Microstructuring of the Catalytic Bed. *Catalysts* **2020**, *10*, 852.
(47) Ordomsky, V. V.; Cai, M.; Sushkevich, V.; Moldovan, S.; Ersen, O.; Lancelot, C.; Valtchev, V.; Khodakov, A. Y. The role of external acid sites of ZSM-5 in deactivation of hybrid CuZnAl/ZSM-5 catalyst for direct dimethyl ether synthesis from syngas. *Appl. Catal., A* **2014**, *486*, 266−275.
(48) Kubas, D.; Semmel, M.; Salem, O.; Krossing, I. Is Direct DME Synthesis Superior to Methanol Production in Carbon Dioxide Valorization? From Thermodynamic Predictions to Experimental Confirmation. *ACS Catal.* **2023**, *13*, 3960−3970.
(49) Krossing, I.; Artamonova, M.; Frei, E. Novel Cu/ZnO-Based Catalysts for the Synthesis of Methanol by CO_2 Hydrogenation. *Z. Anorg. Allg. Chem.* **2012**, *638*, 1566.
(50) Frei, E.; Schaadt, A.; Ludwig, T.; Hillebrecht, H.; Krossing, I. The Influence of the Precipitation/Ageing Temperature on a Cu/ZnO/ZrO_2 Catalyst for Methanol Synthesis from H_2 and CO_2. *ChemCatChem* **2014**, *6*, 1721−1730.
(51) Fehr, S. M.; Nguyen, K.; Njel, C.; Krossing, I. Enhancement of Methanol Synthesis by Oxidative Fluorination of Cu/ZnO Catalysts−Insights from Surface Analyses. *ACS Catal.* **2021**, *11*, 13223−13235.
(52) Vlasenko, N. V.; Kochkin, Y. N.; Telbiz, G. M.; Shvets, O. V.; Strizhak, P. E. Insight into the active site nature of zeolite H-BEA for liquid phase etherification of isobutylene with ethanol. *RSC Adv.* **2019**, *9*, 35957−35968. Published Online: Nov. 5, 2019.
(53) Ladera, R. M.; Fierro, J. L. G.; Ojeda, M.; Rojas, S. TiO_2-supported heteropoly acids for low-temperature synthesis of dimethyl ether from methanol. *J. Catal.* **2014**, *312*, 195−203.
(54) Mota, N.; Millán Ordoñez, E.; Pawelec, B.; Fierro, J. L. G.; Navarro, R. M. Direct Synthesis of Dimethyl Ether from CO_2: Recent Advances in Bifunctional/Hybrid Catalytic Systems. *Catalysts* **2021**, *11*, 411.
(55) da Silva, R. J.; Pimentel, A. F.; Monteiro, R. S.; Mota, C. J. A. Synthesis of methanol and dimethyl ether from the CO_2 hydrogenation over Cu·ZnO supported on Al_2O_3 and Nb_2O_5. *J. CO2 Util.* **2016**, *15*, 83−88.
(56) Bonura, G.; Cannilla, C.; Frusteri, L.; Catizzone, E.; Todaro, S.; Migliori, M.; Giordano, G.; Frusteri, F. Interaction effects between CuO-ZnO-ZrO_2 methanol phase and zeolite surface affecting stability of hybrid systems during one-step CO_2 hydrogenation to DME. *Catal. Today* **2020**, *345*, 175−182.

https://doi.org/10.1021/acsomega.3c00149
ACS Omega 2023, 8, 15203−15216